LABORATORY SCALE PRODUCTION OF LITHIUM MANGANESE OXIDE AS ACTIVE MATERIAL OF LITHIUM-ION BATTERIES IN SOL-GEL METHOD ASSISTED BY LOCAL BIOMASS

PRODUKSI LITIUM MANGAN OKSIDA SKALA LABORATORIUM SEBAGAI BAHAN AKTIF BATERAI ION LITIUM MENGGUNAKAN METODE SOL-GEL DAN BIOMASSA

Muhammad Ilham Bayquni[1], Susanto Sigit Rahardi[*1], Elsy Rahimi Chaldun[2], dan Bambang Sunendar Purwasasmita[3]

[1]Balai Besar Bahan dan Barang Teknik (B4T), Ministry of Industry, Republic of Indonesia, Sangkuriang Street No.14 Bandung City 40135, Indonesia.
[2]Loka Penelitian Teknologi Bersih, Indonesian Institute of Sciences, Kampus LIPI Sangkuriang Street, Bandung City 40135, Indonesia.
[3]Program Studi Teknik Fisika, Institut Teknologi Bandung, Ganesha Street No.10 Bandung City

ABSTRAK

Studi eksperimental dan teoritik produksi litium mangan oksida ($LiMn_2O_4$) dengan metode sol-gel telah dilaksanakan pada skala yang lebih besar daripada penelitian sebelumnya. Maksud dari kajian ini adalah untuk mengevaluasi perilaku bahan selama sintesis yang akan perlu diperhatikan dalam peningkatan skala produksi berbasiskan metode sol-gel. Hasil kalsinasi dianalisis menggunakan TGA dan pembentukan fasa kristal dianalisis menggunakan XRD. $LiMn_2O_4$ fasa spinel mulai terbentuk pada suhu 600^oC. Hasil SEM menunjukkan morfologi butiran yang menarik. Penggembungan volume xerogel yang luar biasa (*swelling*) terjadi ketika pengeringan pada suhu 250^oC to 300^oC. Fenomena eksotermal yang sangat kuat muncul sebagai pemicu swa-bakar yang tidak teratur dan tidak terprediksi selama proses kalsinasi. Kedua fenomena pembesaran xerogel dan eksotermal ini tidak teramati pada xerogel dengan jumlah prekursor yang sedikit. Untuk mengatasi hal tersebut, pengaturan komposisi prekursor dan langkah-langkah tambahan perlu diperhatikan pada saat produksi.

Kata kunci: litium mangan oksida, sol-gel, mekanisme kristalisasi, katoda baterai ion litium

ABSTRACT

Experimental and theoretical studies of the production of lithium manganese oxide ($LiMn_2O_4$) using sol-gel method have been carried out on a larger scale than previous studies. The purpose of this investigation was to observe sample behavior along the synthesis process to be considered in further scale-up production of lithium manganese oxide, based on the sol-gel method. Calcination products were analyzed by TGA and crystalline phase formation analyzed by XRD. $LiMn_2O_4$ spinel phase was formed at 600^oC. SEM showed some interesting morphology. Xerogel swelling was observed overwhelmingly during drying at 250^oC to 300^oC. Exothermic occurrence as a source of irregular and unpredictable auto combustion in the calcination process. Both phenomenon were not observed in a xerogel made with a small amount precursor. Therefore, initial mixture adjustment and additional steps were considered for production.

Keywords: *lithium manganese oxide, sol-gel, crystallization mechanism, lithium ion battery cathode*

INTRODUCTION

Lithium manganese oxide ($LiMn_2O_4$) is a prominent active cathode material of lithium-ion batteries. It has comparable performance with lithium cobalt oxide and relatively cheaper [1]. Research and development of lithium manganese oxide have been carried out extensively over the past 20 years, especially for the recent developments of NMC type material, that more energetic and suitable for ultra-lightweight devices and vehicles powered by batteries [2, 3, 4, 5]. Fortunately Indonesia has substantial local mineral and biomass resources to supply advanced technology materials [6].

As consideration, some research reported convenient methods to synthesize $LiMn_2O_4$, and others approach to specific procedures [7, 8, 9]. Unfortunately, each method has disadvantages such as complicated process, rare material, and some technicality that required complicated processing equipment. Furthermore, few of them explicitly state precursor quantity used in their work. Further investigation needs to consider for an upscale production. As an alternative method, sol-gel method offers several advantages over homogeneous solution as precursors with lower temperature and shorter time [10], particularly in controlling particle morphology and size compared to solid-state material production from homogeneous solution. So far, a few literature reports research on material processing of lithium manganese oxide using the sol-gel method conducted at a high precursor content and the use of biomass as support material.

Sol-gel assisted by chitosan and bacterial cellulose to make high crystalline $LiMn_2O_4$ (JCPDS 35-0782) was reported and showed remarkable battery performance by Rahardi, 2019 [11]. Lithium-ion cell has more endurance during charge-discharge cycles by anisotropic $LiMn_2O_4$ compared to a commercial spherical particle shape.

The pouch type cells were made at the Center for Material and Technical Product (B4T), Ministry of Industry Indonesia, This product complies to an industrial standard and has been patented [12]. Bacterial cellulose is used as a sacrificial bio-template to give growth direction so that the morphology becomes anisotropic. Another sacrificial bio-template is reported using cellulose from starch as a morphology modifier [13,14]. Related to anisotropic structure, chitosan as a template may increase surface area and porosity [15].

In this research, preparation of $LiMn_2O_4$ was conducted in lab-scale with several quantity of precursor. It was considered additional treatments for $LiMn_2O_4$ with high quantity of precursors and possible treatments to overcome detrimental effects due to the excess of some material.

The work of Rahardi was used as a base-method of sol-gel [11]. The effect of a high quantity of precursors, up to seventy-two times higher than the work by Rahardi, was investigated. Thus, the purpose of this research was to study structure analysis, new observable phenomenon, process characteristics, and effect of an extended procedure. Modifications of the base method were also conducted to overcome overwhelming swelling and auto combustion phenomenon along the process. Experiments were carried out with a larger amount than those in the previous research. Hopefully result of this research might be used as an intermediate step for upscaling to commercial production.

MATERIALS AND METHODS

The sol-gel process was carried out in about 100 mL of 1.0 Molar solutions based on [11]. $LiNO_3$ and $MnCl_2$ and ammonia were purchased from MERCK. Technical grade citric acid powder was purchased at the local market Bandung. Chitosan was purchased from Biotech Surindo Cirebon, Indonesia. Aqua destillata was purchased from PT Alkin Global Bandung. Bacterial cellulose (nata de Coco) was purchased at a local firm in Cianjur, West Java, Indonesia.

In general, the procedure consisted of several steps from dissolving precursors in distilled water, making solutions using a stoichiometric molar ratio of $LiNO_3$ and $MnCl_2$ as precursors (Table 1); citric acid (CA) as a chelating agent; chitosan as a template. Followed by the gelling process with stirring solution vigorously for several minutes. Xerogel was dried overnight in an oven. Xerogel was calcined at high temperature with atmosphere of air to form crystal powder of $LiMn_2O_4$.

Table 1. Sample Variation and Weight Loss Along Heat Treatment

Code	Molar Ratio		Total Volume of Sol (mL)	Total Weight Loss (%)			Auto combustion	Notes
	CA	Mn		250°C	400°C	600°C		
P1	3	2	300	8.3	27.9	34.3	around 500°C	base sample
P2	3	2	350	15.2	43.5	63.2	around 500°C	with bacterial cellulose
P3	3	2	1026	-	-	-	500°C	*scale up* and high concentration precursors
P4	3	2	900	2.2	72.05	-	around 500°C	*scale up* of base sample
P5	7	8	1026	75.93	79.28	-	around 500°C	*scale up* and molar ratio adjustment

Initially, we prepared two kinds of samples: P1 as the basic sample and P2 with an addition of bacterial cellulose (see Table 1). In the base method, volume of solution (P1) was about 300 mL. The addition of bacterial cellulose caused an increase in the volume of solution (P2) of about 50 mL. Molar ratio of lithium to manganese to citric acid was 1/2/3. The concentration of total material was 1.0 Molar. Ammonia was used to adjust pH solution at 4.0.

Two samples were made with total concentrations of 8.0 Molar, i.e P3 and P4. Thus, the concentration of precursor in P3 was eight times of that in P1. The total sample material of P3 was about 1 L (exactly 1026 mL). The total material of P4 (900 mL) was three times of P1. Solubility of $MnCl_2$ was considered in the adjusting the concentration in solution. Adjustment of molar ratio was applied to make samples P5, P6 and P7. Extended procedure was applied to P6 and P6 with changing the duration of drying.

Magnetic stirrer hotplate NESCO LAB MS-H280-Pro was used to prepare the solutions, the drying process was done using an oven KBO-600RA, and the calcination process was conducted using a box furnace KOEHLER K24110.

Thermogravimetric and differential thermal analysis (TG-DTA) were carried out to investigate the thermal behavior of samples. TG-DTA analysis was conducted using SETARAM SETSYS-1750 at Center for Ceramics (BBK), Ministry of Industry of Indonesia. The sample was heated in a platinum crucible 100 μL from 50°C to 900°C, at the heating rate of 10 °C/min under air atmosphere.

The structure and phase composition of Lithium manganese powder were determined using the powder XRD technique. The patterns were recorded on an X-ray Diffraction PANalytical X'Pert PRO PW3040/x0 at Center for Geological Survey (PSG), Ministry of Energy and Mineral Resources of Indonesia, using Cu Kα X-ray tube at 1.54060 Å, 40 kV and 30mA with scanning steps of 0.35° (2θ)/min over the 2θ range of 10°–80°. Diffraction patterns were compared with Joint Committee on Powder Diffraction Standards (JCPDS) and using Xpowder program.

The chemical functional groups were examined using a Fourier Transform Infrared Spectrophotometer (FTIR) Shimadzu-Prestige21, *Analytical Instrumentation Laboratory*, *Faculty of Mathematics and Natural Sciences* (FMIPA) ITB. The surface morphology was studied by scanning electron microscopy (SEM) using JEOL-JSM-6510LA, SEM Laboratory at BSCA building of FMIPA, ITB.

RESULTS AND DISCUSSION

Samples P1 and P2 experienced swelling during drying step. Even more, sample P3 with high concentration of bacterial cellulose swelled extremely (Figure 1). These puffy, soft, carbonaceous, and a little bit fibrous xerogels contained volatile gas and vapor. These sample were crushed, dried and subjected to calcination process.

Figure 1. Extreme Swelling of High Concentration Xerogel Sample at Drying 250ºC

Uncontrolled auto-combustion happened to the samples. Specifically, auto combustion of

sample P1 took place between 400°C to 540°C. It was wild and severe heat energy released from the sample. During the auto combustion, crystal coated crucible uniformly and it cannot be taken out of it.

It is quite easy to determine whether lithium manganese oxide formed or not by visual inspection. It appears black-bluish color, whereas manganese oxide usually was dark gray brownish. Small rocky grainy brownish manganese oxide appeared on sample P3 at 250°C, blended with brown caramelized glucose matrix of chitosan.

The black-bluish grainy crystal was always obtained when auto combustion occured. Those grains were large and could not be coated on aluminum substrate because of its coarse particle size (not pass through 200 mesh sieve), while electrode coating process needs particle size of below 400 mesh.

Three different temperatures 675°C (2 h) and 700°C (2 h), and 800°C (10 h) were applied on calcination of sample P1 to produce lithium manganese oxide. The color calcination products were more bluish. Sample P1 with sol phase at pH 5.0 and calcination at 600°C (2 h) also got black-bluish color. It seemed that lithium manganese oxide from above-mentioned conditions have a higher crystalline structure, or there was crystal polymorphism. It was interesting to have further study on the effect of high crystalline structure and polymorphism on battery performance. Nevertheless, all samples exhibited this same phenomenon as the base sample. While the auto combustion, sometime did not occur both in P1 and P2.

Another issue was that samples got highly hygroscopic. Some of them absorbed water from the surrounding air until very wet. It was still hygroscopic, even though it was dried in the oven or heated again. Such powder after drying caused heavy corrosion on the aluminum electrode.

Thermal analysis

Weight loss of sample P1 and P2 obtained by thermogravimetric (with a small quantity of samples), while the other sample obtained from real measurement along the heating process (Table 1). Samples P4 and P5 were undergone auto combusted irregularly and hygroscopic thus far. All of these remarkable phenomena were not observed in our previous study [11].

It was expected that biomass have been decomposed entirely into simpler substance at 400°C. We found two confirmed exothermic regions (marked as **Δ**, Figure 2) of the xerogel of P1: exothermic reactions around 300°C, and intensive exothermic reaction between 400°C and 540°C. These phenomena contributed to auto combustion.

Xerogel of P2 had different behavior (Figure 3). The exothermic reaction was suppressed. Moreover, two exothermic regions such as in P1 merged in P2, making only one region 280°C to 440°C (marked as **Δ**). Cellulose might reduce the exothermic reaction. A substance that causes combustion might had been pacified by its interaction with cellulose. Even though being suppressed, the exothermic energy was still large to influence irregular to sustain auto combustion.

According to DTA result of sample P1, $LiMn_2O_4$ crystal was formed at calcination temperature between 580°C to 710°C. This formation zone was indicated by a slightly flat curve in Figure 2. While in sample P2, the flat curve of $LiMn_2O_4$ formation zone began at a temperature of 500°C (Figure 3). This might indicate that the template provided an initiation of nucleation of crystal at a lower temperature.

Structure analysis

To confirm the formation zone, we investigated sample P1 by XRD (Figure 4). Sample P1 has been calcined at temperature of 600°C for two hours. After phase identification, we found two major phases i.e. 75.3%-weight of $LiMn_2O_4$ (JCPDS 35-0782) and 24.7% of Mn_2O_3 (JCPDS 02-0896). Phase $LiMn_2O_4$ (JCPDS 35-0782) was our target crystal, which was spinel, face-centered cubic crystal structure and space group Fd3m (Table 2). By *Scherrer method*, the crystallite size of $LiMn_2O_4$ P1 were 7 nm (Miller index of 311) and 10 nm (Miller index of 400). These were smaller than the result from base method i.e. 20 nm (Miller index of 311) and 16 nm (Miller index of 400).

To some extent, Miller index 311 and 400 have a significant effect to intercalation/deintercalation of lithium-ion [16]. It is beneficial to reduce crystallite size so that lithium movement is unobstructed by domain boundaries, which presumably allowed fast lithium ion diffusion. The significant differences of crystallite size of each peak indicated anisotropic nature of crystalline. All spinel peaks

shifted slightly to a higher angle. It indicated a smaller lattice parameter, which related to the beginning of calcination process in the formation zone.

The crystal phase of manganese oxide Mn_2O_3 was investigated by XRD on P1 at 560^oC, below its calcination temperature of 600^oC. The temperature was chosen because it was just below the lower limit of the formation

zone, but above its exothermic region. The manganese oxide Mn_2O_3 (JCPDS 02-0896) dominated by 66.1%, together with 33.9% of Mn_2O_3 (JCPDS 33-0900) small crystallite size hexagonal structure (Table 3). According to the observed condition of the hexagonal we inferred that it has a quite mass, and many small domains or possibly grains.
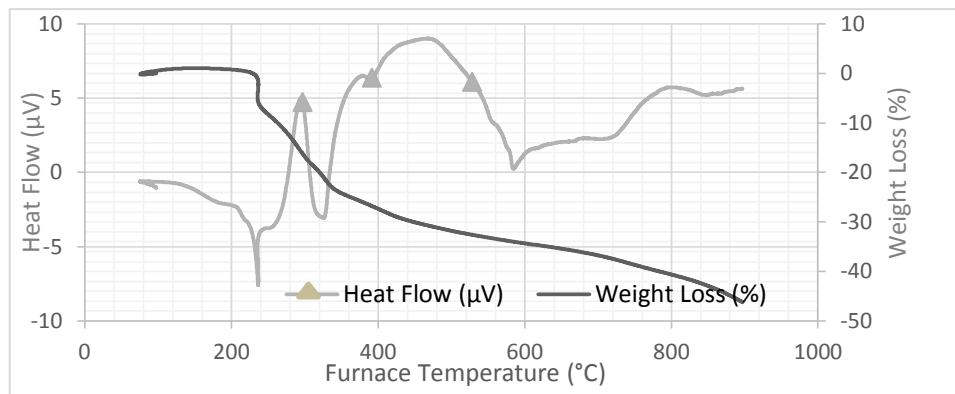

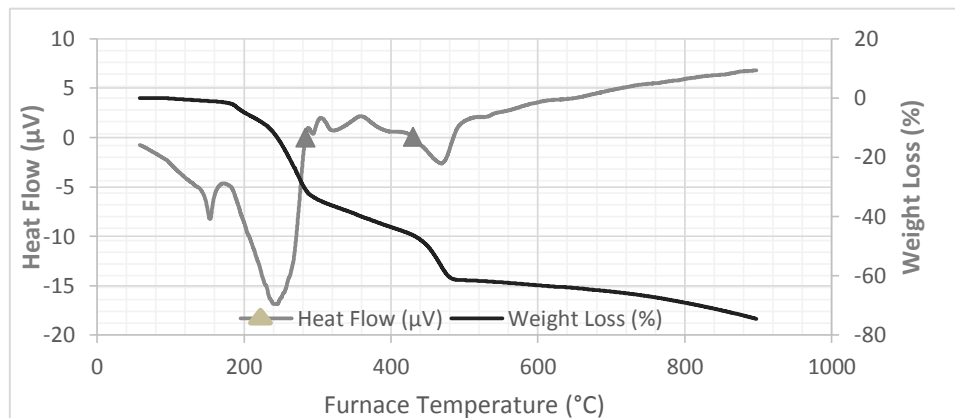**Figure 2.** Thermogravimetric and DTA Curve of Sample P1

Figure 3. Thermogravimetric and DTA Curve of Sample P2

It appeared none of lithium manganese oxide existed at 560^oC (Figure 4). This result confirmed the formation zone. It can be deduced that for sample P1, $LiMn_2O_4$ (JCPDS 35-0782) was transformed from Mn_2O_3 (JCPDS 02-0896). Lithium atoms inserted into the manganese oxide crystal that led to phase transformation from body-centered cubic Ia3 to face-centered cubic Fd3m. We expected that lithium atoms were inside the solids all the time, yet it just contributed to x-ray diffraction pattern when

cubic Fd3m was formed. The cubic Mn_2O_3 (222) was shifted from 33.003 2θ (deg) at 560^oC to 32.940 2θ (deg) at 600^oC. It indicated the lattice stretching of such a plane during the transformation to give space for lithium atoms. The disappearance of the hexagonal at 600^oC indicates that body-centered cubic Mn_2O_3 (JCPDS 02-0896) was transformed from hexagonal Mn_2O_3 (JCPDS 33-0900). The hexagonal lattices were in the stretch condition during transformation.
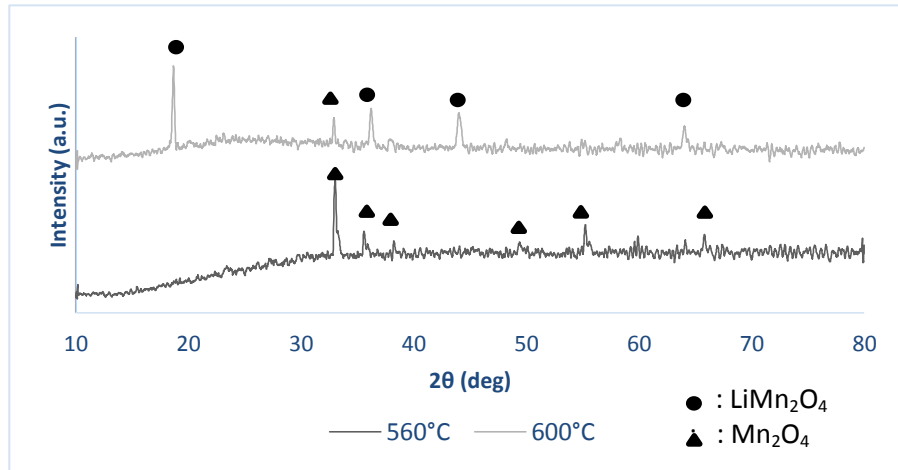
Figure 4. X-Ray Diffraction Pattern of P1

Table 2. Identification of Sample P1 After Calcination Temperature of 600^oC (2 hrs)

JCPDS Number	2θ (deg)	Miller index	Phase	Crystal system, Space group	Crystallite size (nm)	Δθ
35-0782	18.665	111	$LiMn_2O_4$	Cubic, Fd3m	43	0.053
02-0896	32.940	222	Mn_2O_3	Cubic, Ia3	-	0.037
35-0782	36.172	311	$LiMn_2O_4$	Cubic, Fd3m	7	0.086
35-0782	44.010	400	$LiMn_2O_4$	Cubic, Fd3m	10	0.145
35-0782	64.076	440	$LiMn_2O_4$	Cubic, Fd3m	-	0.294

RIR %-weight: $LiMn_2O_4$ (JCPDS 35-0782) = 75.3%; Mn_2O_3 (JCPDS 02-0896) = 24.7%; Δθ was deviation pattern from JCPDS data.

Table 3. Identification of Sample P1 After Calcination Temperature of 560^oC (2 hrs)

JCPDS Number	2θ (deg)	Miller Index	Phase	Crystal system, Space group	Crystallite size (nm)	Δθ
02-0896	33.003	222	Mn_2O_3	Cubic, Ia3	32	0.101
33-0900	35.613	110	Mn_2O_3	Hexagonal axis, -	2	-0.012
02-0896	38.300	400	Mn_2O_3	Cubic, Ia3	4	0.32
02-0896	49.538	431	Mn_2O_3	Cubic, Ia3	87	0.054
02-0896	55.216	440	Mn_2O_3	Cubic, Ia3	3	-0.084
02-0896	65.797	622	Mn_2O_3	Cubic, Ia3	-	0.096

RIR %-weight: Mn_2O_3 (JCPDS 02-0896) = 66.1%; Mn_2O_3 (JCPDS 33-0900) = 33.9%

For further evaluation, the high concentration sample (P3) was calcinated at temperatures of 560^oC and 600^oC (Figure 5). Lithium manganese oxide did not formed in P3 at 600^oC. When it was heated at calcination temperature of 700^oC for two hours, black-bluish color appeared. The formation zone was shifted to a higher temperature. By extrapolation, we estimated the formation zone of sample P3 began around 690^oC.
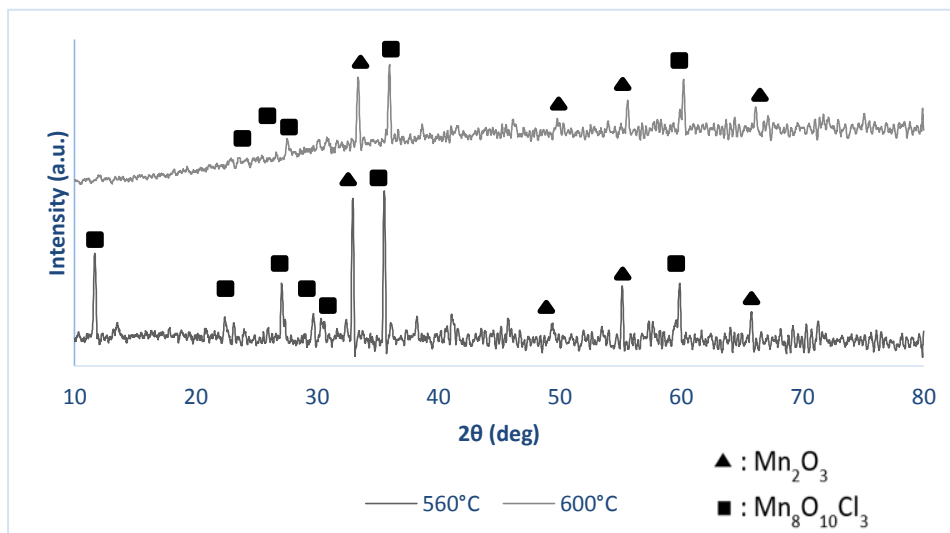
Figure 5. X-Ray Diffraction Pattern of High Concentration Sample (P3)

Table 4. Identification of Sample P3 After Calcination Temperature of $600^{\circ}C$ (2 hrs)

JCPDS Number	2θ (deg)	Miller Index	Phase	Crystal system, Space group	Crystallite size (nm)	$\Delta\theta$
30-0821	27.613	220	$Mn_8O_{10}Cl_3$	Tetragonal, I4/mmm	-	0.482
02-0896	33.442	222	Mn_2O_3	Cubic, Ia3	29	0.541
30-0821	35.973	303	$Mn_8O_{10}Cl_3$	Tetragonal, I4/mmm	26	0.391
02-0896	55.585	440	Mn_2O_3	Cubic, Ia3	-	0.287
30-0821	60.226	336	$Mn_8O_{10}Cl_3$	Tetragonal, I4/mmm	3	0.269
02-0896	66.139	622	Mn_2O_3	Cubic, Ia3	-	0.439

RIR % Weight: Mn_2O_3 (JCPDS 02-0896) = 74.5%; $Mn_8O_{10}Cl_3$ (JCPDS 30-0821) = 25.5%

Table 5. Identification of Sample P3 After Calcination Temperature of $560^{\circ}C$ (2 hrs)

JCPDS Number	2θ (deg)	Miller Index	Phase	Crystal system, Space group	Crystallite size (nm)	$\Delta\theta$
30-0821	11.702	101	$Mn_8O_{10}Cl_3$	Tetragonal, I4/mmm	21	0.006
30-0821	27.096	220	$Mn_8O_{10}Cl_3$	Tetragonal, I4/mmm	-	-0.037
02-0896	32.958	222	Mn_2O_3	Cubic, Ia3	70	0.056
30-0821	35.553	303	$Mn_8O_{10}Cl_3$	Tetragonal, I4/mmm	75	-0.027
02-0896	55.168	440	Mn_2O_3	Cubic, Ia3	5	-0.126
30-0821	59.893	336	$Mn_8O_{10}Cl_3$	Tetragonal, I4/mmm	-	-0.062
02-0896	65.788	622	Mn_2O_3	Cubic, Ia3	-	0.089

RIR % Weight: Mn_2O_3 (JCPDS 02-0896) = 64.1%; $Mn_8O_{10}Cl_3$ (JCPDS 30-0821) = 35.9%

In sample P3 calcinated at temperatures of $560^{\circ}C$ and $600^{\circ}C$, the cubic Ia3 Mn_2O_3 (JCPDS 02-0896) and the tetragonal I4/mmm $Mn_8O_{10}Cl_3$ (JCPDS 30-0821) was formed with different proportion (Table 4 and Table 5). Weight fraction of Mn_2O_3 was higher as calcination temperature increased, whereas $Mn_8O_{10}Cl_3$ was lower. Body-centered cubic Ia3 was transformed from body-centered tetragonal I4/mmm. The peak of $Mn_8O_{10}Cl_3$ at 11.702 2θ (deg) in P3 calcined at $600^{\circ}C$ was disappeared and all planes were in contraction.

Crystallite size Mn_2O_3 of at Miller index of 222 decreased significantly as temperature increased from $560^{\circ}C$ to $600^{\circ}C$. All planes of Mn_2O_3 were in contraction. This circumstances gave a perception that transformation from the former manganese oxides to cubic Ia3 Mn_2O_3 occured in a different mechanism, compared with cubic Ia3 Mn_2O_3 to cubic Fd3m $LiMn_2O_4$.

Morphology analysis

To analyze morphology evolution during calcination, we took SEM images from sample P1 (560°C and 600°C), and sample P3 (560°C and 600°C) as shown in Figure 6.

Figure 6(a) showed sample P1 at temperature of 560°C. There were some rather bulky dodecahedron shapes with very small particles at the surface and surrounded by many rod-like particles. The rod-like particles looked like agglomerated, broken down into small particles, and took shape into dodecahedron. Octahedron spinel (pyramid-like) shapes dominated Figure 6(b). LiMn$_2$O$_4$ crystals were certainly arranged themselves neatly to form octahedron and solidify by crystallization fusion. The surface of some octahedron crystals was very smooth. Both dodecahedron and octahedron are known as the member of cubic or isometric system.
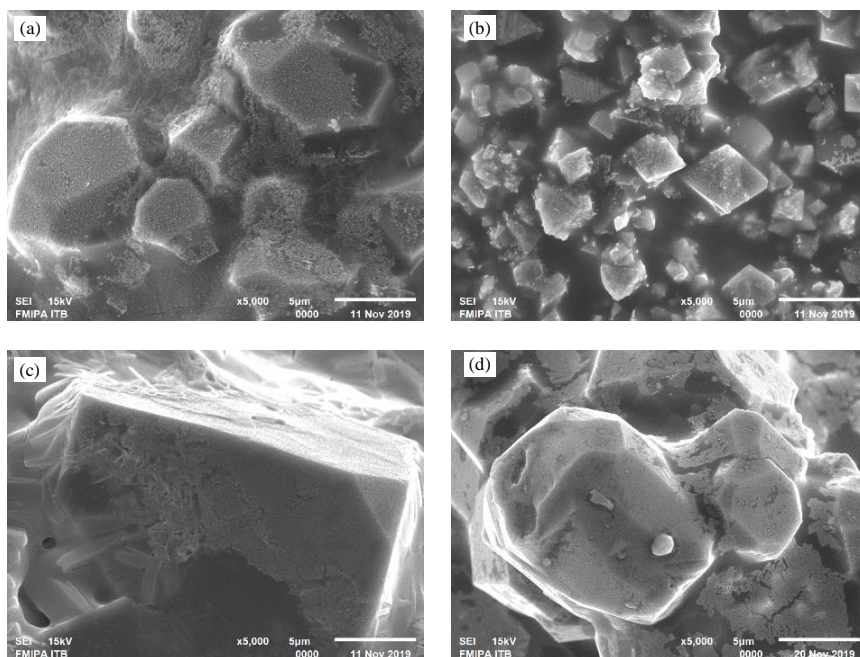

Figure 6. SEM images
(a) P1 calcinated at 560°C. (b) P1 at 600°C. (c) P3 at 560°C. (d) P3 at 600°C

Figure 6(c) indicated the high concentration sample (P3) at temperature of 560°C. It showed fibrous shapes that agglomerated, brokedown into small particles and took shape into truncated cubic. Based on XRD pattern at Figure 5, there were two crystal systems. The truncated cubic was cubic Mn$_2$O$_3$ and fibrous shapes were Mn$_8$O$_{10}$Cl$_3$. The small particles were between 30-80 nm wide (nanocrystals). To form a truncated cubic shape, the small particles transformed from the previous crystal system to the new crystal system, then oriented themselves to form a cubic crystal. Self-assembly arrangement was observed at Figure 6(c). Fibrous and rod-like shapes gave an indication of biomimetic self-assembly oriented attachment (OA) by a previous organic matrix in xerogel. At 600°C, the truncated cube changed to dodecahedron with a rough surface (Figure 6(d)). Based on XRD pattern we inferred dodecahedron was Mn$_2$O$_3$.

It indicated that the truncated cubic was composed of small particles before transforming into another crystal. In some aspect, this phenomenon gave a perception that shares some concept of mesocrystal [17]. Manganese oxides are definitely the intermediates. The formation of mesocrystals are considered non-classical. Overall, we inferred a hypothetical proposition on mechanism during the process. The mechanism comprised continuous processes such as non-classical crystallization, mesocrystal, phase transformation, and crystallization fusion.

Extended procedure

At FTIR data from sample P1 at 540°C, there were absorption at 3423 cm^{-1} (strong-wide) as stretching vibration of OH, and 1631 cm^{-1} (weak-sharp) as bending of it. This indicated that manganese oxide was hydroxylated. The hydroxyls were suspected from citric acid decomposition. This led to the idea that the excess of citric acid played a role as a fuel and gave an undesirable effect in the production.

In adjustment of initial mixture, citric acid had to be decreased to a certain quantity. Citric acid has three carboxyl groups (three lone pairs of electrons) for possible sites for metal cation attachment [18]. Therefore, we took at least one-third of citric acid molar ratio from manganese. If we use EDTA, we could take at least one-fourth of its molar ratio from manganese. On the other side, we extended the duration of drying process. As the result, auto combustion did not happen at sample P6 and P7 (Table 6). If chitosan was half from the previous quantity, auto combustion happened again at sample P7. The chitosan suppressed citric acid combustion. Heating with less-oxygen furnace chamber condition at exothermic regions helped to reduce the occurrence of auto combustion, as fuel were already decomposed at 540°C.

An additional post-treatment procedure such as washing and drying eliminated excess substance, such as carbonyls that caused hygroscopicity of powder. After manual grinding, samples P1, P6, and P7 passed 400 mesh sieve, these samples were not hygroscopic and ready for electrode production as compared with dehydroxylation methods [19].

Table 6. Results of Treatment on Modified P1

Sample Code	Molar Ratio		Total Weight Loss (%)			Auto combustion	Notes
	CA	Mn	250°C	400°C	600°C		
P1	3	2	8.3	27.9	34.3	Yes, around 500°C	base sample
P6	3	2	51.65	82.63	83.66	No	with extended duration of drying
P7	1	3	60.22	63.68	68.78	No	with molar ratio adjusting

CONCLUSION

Lithium manganese oxide successfully synthesized in the lab-scale condition, with increasing the amount of raw material three times from the base sample and adjustment of composition. It was observed that crystal formation from manganese oxide to LiMn$_2$O$_4$ took place at the beginning of its formation zone. The formation of manganese oxide went long before the formation of LiMn$_2$O$_4$. Using of templates lead to formation zone shift to a lower temperature, whereas high concentration was on the contrary. The mechanism comprised continuous processes such as non-classical crystallization, mesocrystal, phase transformation, and crystallization fusion. The extended procedure reduced severe hygroscopicity, overwhelming swelling, and also auto combustion. Results of this research gave insight on how to control and manipulate the process of lithium manganese oxide production based on a previous method with an increase of production capacity.

ACKNOWLEDGMENTS

REFERENCES

[1] Naresh Susarla; Shabbir Ahmed, "Estimating the Cost and Energy Demand of Producing Lithium Manganese Oxide for Li-Ion Batteries," *Alexandria*, 2020.

[2] A. R. Armstrong and P. G. Bruce, "Synthesis of Layered LiMnO2 as an Electrode for Rechargeable Lithium Batteries.pdf." *Nature*, pp. 499–500, 1996.

[3] Y. Sun, "Synthesis of Spinel LiMn$_2$O$_4$ by the Sol - Gel Method for a Cathode-

Active Material in Lithium Secondary Batteries," *Am. Chem. Soc.*, pp. 4839–4846, 1997.

[4] M. M. Thackeray and M. H. Rossouw, "Synthesis of Lithium-Manganese-Oxide Spinels: A Study by Thermal Analysis," *J. Solid State Chem.*, pp. 441–443, 1994.

[5] O. Toprakci, H. A. K. Toprakci, Y. Li, L. Ji, L. Xue, and H. Lee, "Synthesis and Characterization of x Li_2MnO_3.(1-x)LiMn1/3Ni1/3Co1/3O2 Composite Cathode Materials for Rechargeable Lithium-Ion Batteries," *J. Power Sources*, vol. 241, pp. 522–528, 2013.

[6] A. Supriadi *et al.*, *Kajian Dampak Hilirisasi Mineral Mangan Terhadap Perekonomian Regional*. Jakarta: Pusat Data dan Teknologi Informasi Energi dan Sumber Daya Mineral, 2017.

[7] J. Jiang *et al.*, "Synthesis of $LiMn_2O_4$ Nanoparticles Using Nano-Sized MnO_2 Precursor and Their Electrochemistry Performance," *J. Nanosci. Nanotechnol.*, vol. 16, no. 12, pp. 12640–12643, 2016.

[8] S. Geng, S. Geng, and Y. Zhai, "Synthesis of $LiMn_2O_4$ via High Temperature Ball Milling Process," *Mater. Manuf. Process.*, vol. 6914, no. April, 2017.

[9] M. Lee, S. Lee, P. Oh, Y. Kim, and J. Cho, "High Performance $LiMn_2O_4$ Cathode Materials Grown with Epitaxial Layered Nanostructure for Li-Ion Batteries," *Am. Chem. Soc.*, vol. 14, pp. 993–999, 2014.

[10] A. E. Danks, S. R. Hall, and Z. Schnepp, "The Evolution of Sol-Gel Chemistry as A Technique for Materials Synthesis," *Mater. Horizons*, vol. 3, pp. 91–112, 2016.

[11] S. S. Rahardi, "Sintesis Litium Mangan Oksida Melalui Metode Sol Gel dengan Bio Template Selulosa Bakteri Sebagai Bahan Katoda Baterai Ion Litium (Thesis Master)," Institut Teknologi Bandung, 2016.

[12] S. S. Rahardi, "Sintesis, Sreparasi Bahan Katoda Anisotropik, Sel Baterai Ion Litium dan Pengembangannya," 2019/04488, 2019.

[13] Balai Besar Bahan dan Barang Teknik, "Laporan Kegiatan Penelitian - Kajian Teknologi Batere Mobil Listrik LCGC," Bandung, 2013.

[14] S. S. Rahardi, A. H. Daulay, S. Hidayatullah, and B. S. Purwasasmita, "Pengembangan Sintesis Serbuk Lithium Manganat untuk Bahan Katoda Batere Lithium Ion," *Pros. Semin. Nas. Keramik XII*, 2013.

[15] A. Wibowo, R. F. Indrawan, L. A. T. Wulan Asri, S. S. Rahardi, and B. S. Purwasasmita, "The Influence of Chitosan Concentration on Morphology and Conductivity of Lithium Aluminium Titanate Phosphate for Solid Electrolytes of Lithium-Ion Battery Application," *IOP Conf. Ser. Mater. Sci. Eng.*, vol. 509, no. 1, 2019.

[16] M. Bianchini, F. Fauth, E. Suard, J.-B. Leriche, C. Masquelier, and L. Croguennec, "Spinel materials for Li-ion batteries: new insights obtained by operando neutron and synchrotron X-ray diffraction," *Energy Mater.*, pp. 1–14, 2015.

[17] F. Dang, T. Hoshino, Y. Oaki, E. Hosono, H. Zhou, and H. Imai, "Synthesis of Li-Mn-O Mesocrystals with Ccontrolled Crystal Phases Through Topotactic Transformation of MnCO3," *Nanoscale*, vol. 5, no. 6, pp. 2352–2357, 2013.

[18] N. A. F. Abdullah and L. S. Ang, "Binding sites of Deprotonated Citric Acid and Ethylenediaminetetraacetic Ccid in the Chelation with Ba2+, Y3+, and Zr4+ and Their Electronic Properties: A Density Functional Theory Study," *Acta Chim. Slov.*, vol. 65, no. 1, pp. 231–238, 2018.

[19] C. Ivander, M. I. Bayquni, and S. Rahardi, "Dehidrasi dan Dehidroksilasi Litium Mangan Oksida dari Metode Sol-Gel untuk Elektroda Baterai Ion Litium," in *Seminar Nasional B4T*, 2020.